Multiple scattering effect in acoustic response from a bubble cloud

Alexei Kouzoubov

Maritime Division, Defence Science and Technology Group, Edinburgh, Australia

ABSTRACT

An implementation of the acoustic multiple scattering between bubbles in a bubble cloud to model the cloud response to an active sonar signal is described. The bubble cloud is modelled as an aggregation of identical omnidirectional point scatterers. The acoustic scattering strength of the scatterers is calculated from the physical properties of bubbles. The dependence of the multiple scattering effect on air volume fraction, sonar frequency, and the bubble size is investigated.

1 INTRODUCTION

Modern simulations of sonar performance in military applications require higher fidelity models of sonar echoes from underwater objects. Various bubbly wakes play an important part in these simulations. Examples include surface ship wakes, exhaust gas bubbles behind a torpedo, the bubble cloud created by an underwater explosion. All of them can be described as bubble clouds of certain shape with a certain size and spatial distribution of bubbles. All these parameters define how a signal from an active sonar will be scattered by a bubble cloud. Previously, a high-fidelity model of scattering of an acoustic wave from a bubble cloud has been developed in a single-scattering approximation (Kouzoubov 2017). One of the main characteristics of the wakes is the air volume fraction, or bubble density. It can be very high at the initial stages of the wakes, gradually falling to very low values as the wake develops. When the bubble density is high, the scattering of acoustic wave between the bubbles, in other words multiple scattering, can contribute to the overall backscattered sonar signal from a bubbly wake. In this paper we investigate how multiple scattering of acoustic wave in bubble clouds affects the return signal, and in what degree it depends on the air volume fraction.

2 MODEL DESCRIPTION

The simulation of multiple scattering effect presented in this paper is based on the approach described in several papers (Hahn 2007, Mookerjee and Dowling 2015, 2017), which are, in their turn, based on an early paper of Foldy (Foldy 1945). For completeness, we reproduce here the main assumptions and equations of this approach to multiple scattering. Unlike previous work (Kouzoubov 2017), we do not consider scattering of a sonar pulse of finite length but rather scattering of a continuous plane wave. We consider an ensemble of N scatterers at positions $\vec{r}_i$. The simulation is simplified by the assumption that the scatterers are identical and omnidirectional. The total pressure field at a point of observation $\vec{r}$ can be written as the sum of an incoming field $p_0(\vec{r})$ and a scattered field $p_s(\vec{r})$

$$p(\vec{r}) = p_0(\vec{r}) + p_s(\vec{r}) = p_0(\vec{r}) + \sum_{i=1}^{N} f_s p^i(\vec{r}_i) G(k; \vec{r} - \vec{r}_i) \tag{1}$$

In the above equation $p^i(\vec{r}_i)$ is the field incident on ith scatterer, f_s is the complex scattering coefficient, G is the Green's function

$$G(k; \vec{r}_i - \vec{r}_j) = \frac{e^{ik|\vec{r}_i - \vec{r}_j|}}{|\vec{r}_i - \vec{r}_j|} \tag{2}$$

The field incident on the ith scatterer is the sum of the incoming field $p_0(\vec{r})$ at the position $\vec{r} = \vec{r}_i$ and the scattered field generated by all other scatterers propagated to the position $\vec{r}_i$:

$$p^i(\vec{r}_i) = p_0(\vec{r}_i) + \sum_{\substack{j=1 \\ j \neq i}}^{N} f_s p^j(\vec{r}_j) G(k; \vec{r}_i - \vec{r}_j) \tag{3}$$

The equations (1) and (3) form a set of N linear equations. The solution of these equations for the scattered field can be written in $N \times N$-matrix form:

$$p_s(\vec{r}) = f_s[(\mathbf{1} - f_s\boldsymbol{G}^k)^{-1}\boldsymbol{p}_0]^T \cdot \boldsymbol{G}^k(\vec{r}), \tag{4}$$

with the matrix $\boldsymbol{G}^k$ defined as

$$\boldsymbol{G}^k_{i,j} = \begin{cases} G\left(k; \vec{r}_i - \vec{r}_j\right), & i \neq j \\ 0, & i = j, \end{cases} \tag{5}$$

with the vectors $\boldsymbol{p}_{0i}$ and $\boldsymbol{G}^k(\vec{r})$ **defined** as

$$\boldsymbol{p}_{0i} = p_0(\vec{r}_i), \tag{6}$$

$$\boldsymbol{G}^k(\vec{r}) = G(k; \vec{r}_i - \vec{r}). \tag{7}$$

The above solution was implemented in MATLAB. It is obvious that the time to solve the multiple scattering equations depends on the number of scatterers. Figure 1 shows the results of a numerical test for estimating the time required to solve the equation. For each number of scatterers, 1000 random realizations of their positions were generated and the solution was timed at every realization. The mean values of the solution time are shown in the figure. The error bars indicate the standard deviation of the solution time distribution. The results presented in the figure were obtained on a 64-bit computer with a single Intel® Xeon® CPU E5-2667 v3 @ 3.20 GHz. The computer RAM was 64 GB, but only about 3 GB were used by the code at the maximum number of scatterers of 3000. The plot shows that the solution time is reasonable at the relatively large number of scatterers.

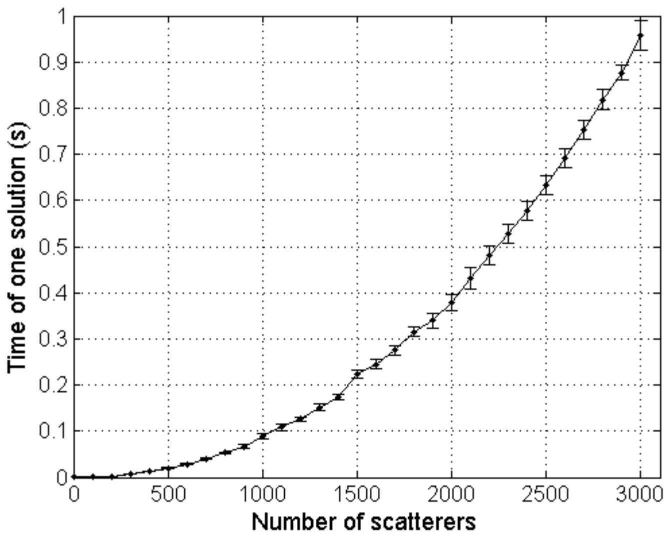

Figure 1. Average time of MATLAB implementation of solution of equation (4). Averaged over 1000 random realizations of scatterers' positions.

To verify our implementation we reproduce results published in (Mookerjee and Dowling 2017) on the so-called Coherent Backscatter Enhancement (CBE). CBE occurs when an aggregation of many individual scatterers is insonified by an incident acoustic plane wave. It reveals itself in the form of a peak in the angular distribution of backscattered intensity in the direction opposite to the propagation direction of the incident wave (Mookerjee and Dowling 2017). It depends on many parameters, such as shape of the aggregation, its size, the acoustic strength and density of individual scatterers in the aggregation. The paper (Mookerjee and Dowling 2017) provides details of CBE dependence on various parameters. Here we reproduce only a specific case of backscattering from a spherical cluster of point scatterers, which is illustrated in Figure 2. It is described by three non-dimensional parameters: $ka, ks,$ and $k\sigma_s^{1/2}$, where $k = 2\pi f/c$ is the acoustic wave number with f being the acoustic wave frequency and c the speed of sound, a is the aggregation radius, s is the average spacing between scatterers, and σ_s is a scatterer's cross section. In this example we used the following values of the parameters: $ka = 16$ and 25, $ks = 3.2$, and $k\sigma_s^{1/2} = 1.5$, which correspond to some cases considered in (Mookerjee and Dowling 2017).

The wave-number-scaled scattering coefficient, kf_s, can be calculated in the elastic scattering approximation as (Mookerjee and Dowling 2015):

$$kf_s = k\sqrt{\sigma_s}\left[\left(\frac{1}{4\pi} - \left(\frac{k\sqrt{\sigma_s}}{4\pi}\right)^2\right)^{1/2} - i\frac{k\sqrt{\sigma_s}}{4\pi}\right] \tag{8}$$

More accurately, in the specific case of bubbles the scattering coefficient can be calculated from the following expression (Medwin and Clay 1998):

$$f_s = \frac{R_b}{\left[\left(\frac{f_R}{f}\right)^2 - 1\right] - i\delta}, \tag{9}$$

where the total damping constant

$$\delta = \delta_r + \delta_t + \delta_v \tag{10}$$

is the sum of the reradiation term $\delta_r = kR_b$, the thermal damping term $\delta_t = (d/b)(f_R/f)^2$, and the viscous damping term $\delta_v = 4\mu/(2\pi f \rho_A R_b^2)$, where μ is the dynamic viscosity of the ambient fluid, ρ_A is its density. The resonance frequency of the bubble, f_R, is calculated according to the following equation (Medwin and Clay 1998):

$$f_R = \frac{1}{2\pi R_b}\sqrt{\frac{3\gamma b\beta p_A}{\rho_A}} \tag{11}$$

In the above equation the parameters b and β are defined as (Medwin and Clay 1998):

$$\beta = 1 + \frac{2\sigma}{p_A a}\left(1 - \frac{1}{3\gamma b}\right), \tag{12}$$

$$b^{-1} = \left[1 + \left(\frac{d}{b}\right)^2\right]\left[1 + \left(\frac{3\gamma - 3}{X}\right)\left(\frac{\sinh X - \sin X}{\cosh X - \cos X}\right)\right], \tag{13}$$

$$\frac{d}{b} = 3(\gamma - 1)\left[\frac{X(\sinh X + \sin X) - 2(\cosh X - \cos X)}{X^2(\cosh X - \cos X) + 3(\gamma - 1)X(\sinh X - \sin X)}\right], \tag{14}$$

$$X = a\left(\frac{2\omega\rho_g C_{pg}}{K_g}\right)^{1/2}. \tag{15}$$

The scattering cross-section of an individual bubble is given by the following equation (Medwin and Clay 1998):

$$\sigma_s = \frac{4\pi R_b^2}{\left[\left(\frac{f_R}{f}\right)^2 - 1\right]^2 + \delta^2} \tag{16}$$

While generating a spherical aggregation of randomly placed scatterers (Figure 2), it was made certain that the minimum distance between individual scatterers satisfied the following condition: $ks_{min} > 1.6$. The minimum spacing prevents numerical singularity problems arising from the form of Green's function (2). This certainly excludes very high air volume fractions from consideration. It should be noted here that, in the case of very dense clouds, the form of equations (1) and (2) may not be valid anyway. The results for normalized mean square pressure $\langle|p_s(\phi)|^2\rangle/\langle|p_s(0)|^2\rangle$ versus scattering angle ϕ in degrees are presented in Figure 3. The averaging was performed over 10000 random realizations of spherical aggregation for $ka = 16$ and 7000 realizations for $ka = 25$. To ensure the far-field conditions, the distance from the source and receiver to the center of the agglomerate of scatterers was chosen as $R_{rt} \approx 70ka^2$. One can see a characteristic CBE peak, similar to that shown in FIG 2 of (Mookerjee and Dowling 2017). This verifies our implementation of the multiple scattering solution from an aggregation of point scatterers of the same acoustic strength.

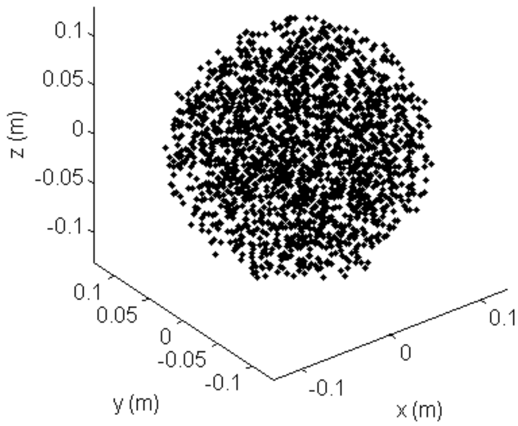

Figure 2. Example of spherical aggregation of individual scatterers. In this example, $v_f = 10^{-3}, kR_b = 0.4, f = 100\ kHz$.

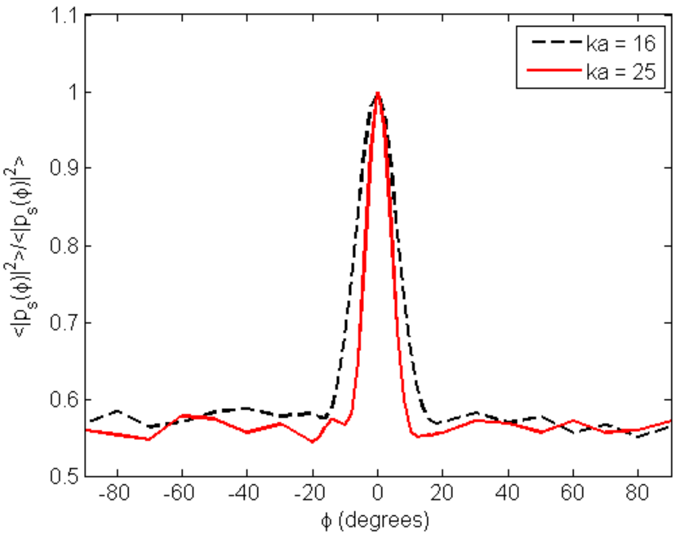

Figure 3. Normalized mean square pressure $\langle|p_s(\phi)|^2\rangle/\langle|p_s(0)|^2\rangle$ versus scattering angle ϕ in degrees.

3 RESULTS AND DISCUSSION

Using the implemented model of multiple scattering from an aggregation of monodisperse individual scatterers, we now investigate how the multiple scattering effects depend on the volume fraction of gas bubbles in a cloud. We use for this purpose two types of aggregations of point scatterers: spherical (Figure 2) and an element of a sonar conical beam (Figure 6). Although we do not simulate a bubble cloud response to a finite sonar pulse, we can consider the response by a volume of the cloud insonified by such a pulse to a plane continues wave.

Consider N bubbles in a spherical bubble cloud (Figure 2). The bubbles are assumed to be of the same volume $V_b = \frac{4}{3}\pi R_b^3$, where R_b is the bubble radius. The air volume fraction in a spherical bubble cloud is

$$v_f = \frac{NV_b}{V_{bc}}, \tag{17}$$

where $V_{bc} = \frac{4}{3}\pi R_{bc}^3$ is the volume of the spherical bubble cloud with radius R_{bc}. The average distance between bubble centres can be estimated as

$$s = \left(\frac{V_{bc}}{N}\right)^{\frac{1}{3}} \tag{18}$$

Substituting V_{bc} from (17) and multiplying both sides of equation (18) by the wave number k, we will get the following relation between non-dimensional parameters:

$$ks = kR_b\left(\frac{4\pi}{3v_f}\right)^{\frac{1}{3}} \tag{19}$$

In the following calculations we assume that the number of bubbles, N, in the spherical cloud is the same for different bubble sizes. From this, the non-dimensional radius of the cloud is

$$kR_{bc} = ks\left(\frac{3N}{4\pi}\right)^{\frac{1}{3}} = kR_b\left(\frac{N}{v_f}\right)^{\frac{1}{3}} \tag{20}$$

In the following calculations we set $N = 2000$. The non-dimensional bubble radius, kR_b, was varied in the interval from 0.4 to 2 with a step of 0.2. The air volume fraction values were 10^{-4}, 10^{-3}, $2 \cdot 10^{-3}$, $3 \cdot 10^{-3}$, and $4 \cdot 10^{-3}$. This provided the minimum value of non-dimensional average distance between bubble $ks \approx 4$, which simplified the generation of a random realization of bubbles with the condition $ks \geq 1.6$. As in the previous section, to ensure the far-field conditions the distance to source and receiver was chosen as $R_{rt} \approx 70kR_{bc}^2$. The scattering strength of individual bubbles at chosen parameters is shown in Figure 4. In this figure, the black curve is the scattering strength in the wide range of non-dimensional bubble sizes, the magenta circles represent the scattering strength at the specified values of the non-dimensional bubble size. It can be seen that the chosen values are well above the resonant bubble size.

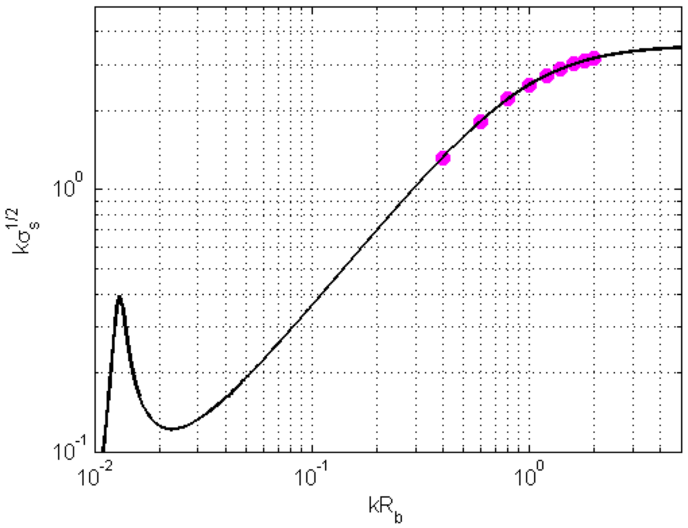

Figure 4. Non-dimensional scattering strength of individual bubbles: black curve – in the wide range of the non-dimensional bubble sizes, magenta circles – at the specified values of the non-dimensional bubble size.

For given values of non-dimensional bubble size kR_b and bubble volume fraction v_f we generate N_k random realizations of a spherical agglomerate of individual scatterers. For each realization we calculate the multiple scattering pressure, p_{ms}, and the single scattering pressure, p_{ss}. Figure 5 shows the ratio $\langle|p_{ms}|^2\rangle/\langle|p_{ss}|^2\rangle$, where angle brackets define averaging over N_k random realizations. In these simulations, $N_k = 5000$. One can see from the figure that the ratio is increasing with decreasing scaled bubble size, kR_b, and increasing volume fraction, v_f.

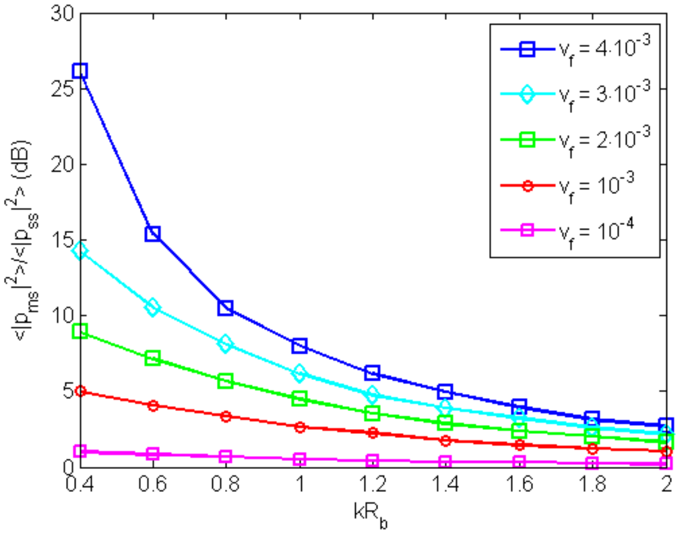

Figure 5. Ratio of multiple scattered intensity to the single scattered intensity for the case of spherical aggregation of monodisperse bubbles for various air volume fractions.

Apparently there are two competing factors influencing the magnitude of the multiple scattering effect: the scattering strength of individual bubbles, $k\sigma_s^{1/2}$, and the average distance between them, ks. Obviously, from equation (2), the less distance between the bubbles, the higher scattered pressure from a bubble reaching other bubbles. This results in an increase of total scattered pressure from an agglomerate of scatterers. As we see from equation (19), a decrease of the bubble size and an increase of the volume fraction leads to a decrease of the average distance between the bubbles. On the other hand, from Figure 4 we see that a decrease of bubble size also results in a decrease of the scattering strength of an individual bubble. Apparently, this influences the effect of multiple scattering to a lesser degree than the average distance between the bubbles.

Another shape of agglomerate of scatterers that we consider here is an ensemble of scatterers in a volume insonified by a sonar pulse (Figure 6). Such a volume element was considered in previous work (Kouzoubov 2017) for the case of single scattering. Assuming a conical beam with the beam angle γ, the insonified volume at the distance r from the sonar can be calculated according to the following equation:

$$V = \frac{1}{3}\pi \tan^2\left(\frac{\gamma}{2}\right)\left\{\left(r + \frac{1}{4}c\tau\right)^3 - \left(r - \frac{1}{4}c\tau\right)^3\right\}, \tag{21}$$

where τ is the pulse length and c is the speed of sound in water. Here we consider the same values of kR_b and v_f as in the case of the spherical agglomerate of bubbles. Again, the number of scatterers was assumed to be the same for all combinations of the above parameters, $N = 2000$, and the geometrical parameters of the insonified volumes are calculated from the values of kR_b, v_f, and N. The average distance between the bubbles is defined by the same equation (19). Using the approximate form of equation (21):

$$V = \frac{\pi}{2}c\tau\left(\frac{r\gamma}{2}\right)^2, \tag{22}$$

and defining the characteristic size of the insonified volume as the radius of the beam in the middle section of the volume:

$$R_{bc} = \frac{r\gamma}{2}, \tag{23}$$

we will find that

$$kR_{bc} = \left(\frac{2(ks)^3 N}{\pi kc\tau}\right)^{1/2}. \tag{24}$$

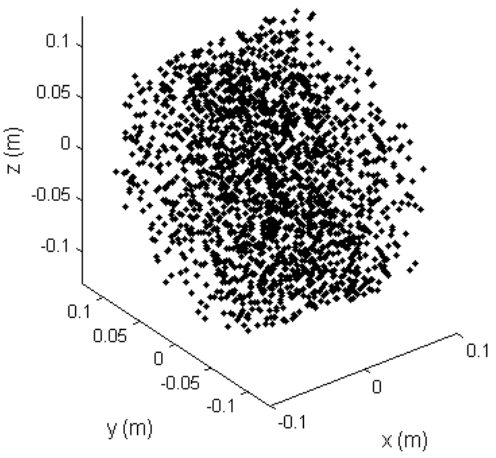

Figure 6. Insonified beam element illustration. In this example, $v_f = 10^{-3}, kR_b = 0.4, f = 100\ kHz$.

As in the case of a spherical cluster, we generate N_k random realizations of bubble positions within the insonified volume for given values of the non-dimensional bubble size, kR_b, and the air volume fraction, v_f. For each realization we calculate the multiple scattering pressure, p_{ms}, and single scattering pressure, p_{ss}. Figure 7 shows the ratio $\langle|p_{ms}|^2\rangle/\langle|p_{ss}|^2\rangle$, where angle brackets define averaging over N_k random realizations. In these simulations, $N_k = 5000$. We can see that the results are even quantitatively similar to those for the spherical cloud of bubbles (Figure 5), which confirms that solutions for both shapes of volumes were obtained in the far-field.

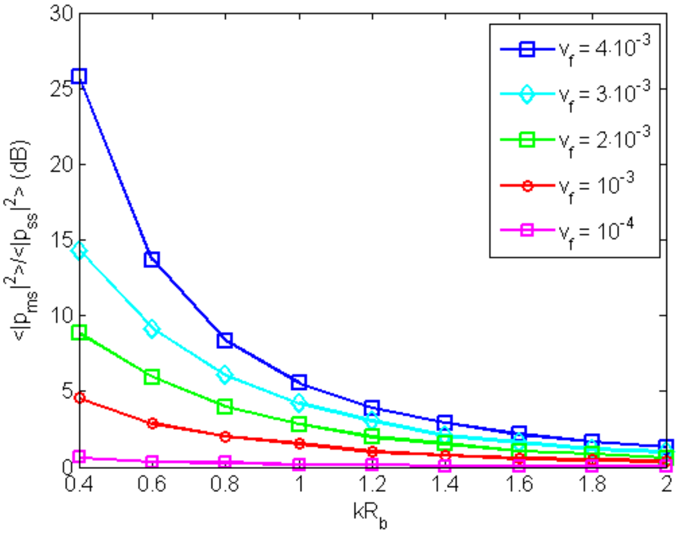

Figure 7. Ratio of multiple scattered intensity to the single scattered intensity for the case of a beam element filled with monodisperse bubbles for various air volume fractions.

4 CONCLUSION

A mathematical technique for calculating acoustic backscattering from a bubble cloud of identical bubbles has been implemented in Matlab. The technique takes into account multiple scattering between bubbles, which allowed us to investigate the dependence of multiple scattering effects on the gas volume fraction in a bubble cloud. It was found that the multiple scattering takes significant effect for the volume fraction higher than 10^{-3}. In practical cases of surface ship wakes the volume fraction is usually lower especially in the far wake region (Stanic et al. 2009), which is of most interest for the considered type of applications.

REFERENCES

Foldy, L. L. 1945. "The multiple scattering of waves. I. General theory of isotropic scattering by randomly distributed scatterers." *Physical Review* no. 67:107-119.

Hahn, T. R. 2007. "Low frequency sound scattering from spherical assemblages of bubbles using effective medium theory." *Journal of the Acoustical Society of America* no. 122 (6):3252-3267. doi: DOI: 10.1121/1.2793610.

Kouzoubov, A. 2017. "Monte Carlo model of acoustic response from a bubble cloud." In.: Proceedings of ACOUSTICS 2017 Perth: Sound, Science and Society - 2017 Annual Conference of the Australian Acoustical Society, AAS 2017. Accession Number: edselc.2-52.0-85041342505

Medwin, H, and CS Clay. 1998. *Fundamentals of acoustical oceanography*. Sydney: Academic Press.

Mookerjee, A., and D. R. Dowling. 2015. "Simulating acoustic coherent backscattering enhancement from random aggregations of omnidirectional scatterers." *Journal of the Acoustical Society of America* no. 138 (2):758-768. doi: http://dx.doi.org/10.1121/1.4927032.

Mookerjee, A., and D. R. Dowling. 2017. "Far-field coherent backscatter enhancement from random aggregations of scatterers and comparisons to backscattering from single isolated spheres." *Journal of the Acoustical Society of America* no. 141 (2):1214-1225. doi: DOI: 10.1121/1.4976075.

Stanic, S., J. W. Caruthers, R. R. Goodman, E. Kennedy, and R. A. Brown. 2009. "Attenuation measurements across surface-ship wakes and computed bubble distributions and void fractions." *IEEE Journal of Oceanic Engineering* no. 34 (1):83-92. doi: http://dx.doi.org/10.1109/JOE.2008.2008411.